Non-linear dissolution mechanisms of sodium calcium phosphate glasses as a function of pH in various aqueous media

Reece N. Oosterbeek[a,*], Kalliope I. Margaronis[a], Xiang C. Zhang[b], Serena M. Best[a], Ruth E. Cameron[a,*]

[a] *Cambridge Centre for Medical Materials, Department of Materials Science and Metallurgy, University of Cambridge, Cambridge, United Kingdom*
[b] *Lucideon Ltd, Queens Road, Penkhull, Stoke-on-Trent, United Kingdom*

Abstract

Phosphate glasses for bioresorbable implants display dissolution rates that vary significantly with composition, however currently their mechanisms of dissolution are not well understood. Based on this systematic study we present new insights into these mechanisms.

Two-stage dissolution was observed, with time dependence initially parabolic and later linear, and a two-stage model was developed to describe this behaviour. Dissolution was accelerated by lower Ca concentration in the glass, and lower pH in the dissolution medium.

A new dissolution mechanism is proposed, involving an initial stage where diffusion-controlled formation of a conversion layer occurs. Once the conversion layer is stabilised, layer dissolution reactions become rate-limiting. Under this mechanism the transition time is sensitive to the nature of the conversion layer and solution conditions.

These results reveal the dependence of P_2O_5-CaO-Na_2O glass dissolution on solution pH, and provide new insight into the dissolution mechanisms, particularly regarding the transition between the two dissolution stages.

Keywords: Phosphate glass, Calcium-phosphate glass, Dissolution behaviour, Dissolution rate, Dissolution mechanism

1. Introduction

Phosphate-based glasses are attractive materials for medical implants, due in part to their cytocompatibility and demonstrated potential for use in soft tissue applications such as ligament and muscle scaffolds, wound healing, and promoting angiogenesis [1–5]. However perhaps their greatest advantage is their solubility in aqueous solutions, and the ability to tune this solubility over many orders of magnitude by tailoring the glass composition, to match the degradation lifetime of the material with tissue repair [6]. Phosphate glasses have potential applications including hard tissue engineering, as well as controlled release and antimicrobial materials [7, 8], and can also be combined with polymers in fully degradable polymer-glass composites for hard or soft tissue implant materials [2, 9–13]. The biological response of these materials is often closely linked to the dissolution rate of the glass - in order to support cell adhesion and survival, the surface must dissolve slowly enough to allow physical bonding [2, 12–14]. It is clear that in any application, the degradation timescale of the material is of critical importance, therefore intimate knowledge of the dissolution behaviour of the phosphate glass is crucial.

Due to their similarity in composition to natural bone, calcium containing phosphate glasses are of particular interest for medical applications. Early work by Bunker et al. and Uo et al. [15, 16] found that Ca

*Corresponding author
Email addresses: rno23@cam.ac.uk (Reece N. Oosterbeek), rec11@cam.ac.uk (Ruth E. Cameron)

ions introduced within the glass form ionic crosslinks between non-bridging oxygens of two different glass chains [17], enhancing the chemical durability. Later work has shown Mg and Fe to have a similar, even stronger effect [6, 18, 19], with crosslinking of non-bridging oxygens by di- and tri-valent metal ions having a dominant effect on the physical properties, including dissolution rate, density, and T_g. The pH dependence of Ca-P glass dissolution has not been extensively studied, however results in similar systems such as Zn-P and Na-P glasses indicate that the rate of dissolution increases in acidic or basic solutions [15, 20, 21], with acidic solutions accelerating dissolution by disrupting ionic crosslinks between phosphate chains.

Despite having been the subject of research for several decades, uncertainty remains over the mechanisms occurring during phosphate glass dissolution. Several studies [7, 15, 22] have observed an initial dissolution stage with parabolic time dependence, in P_2O_5-CaO-Na_2O glasses, which Bunker et al. attributed to water diffusion and formation of a surface hydration layer [15]. This initial stage has also been observed in P_2O_5-FeO-Fe_2O_3-Na_2O glasses [23], however other works on P_2O_5-CaO-Na_2O glasses have not observed this initial non-linear stage [18, 21], suggesting that it may be related to the changing ionic strength of the solution rather than diffusion and ion exchange [24]. The later stage of dissolution, with linear time dependence, is considered to be controlled by the reaction of the hydrated layer at the glass-solution interface [22–24]. The cause of the transition between these stages is not yet well understood, but the transition time has been observed to be roughly correlated to the durability of the glass [15] (i.e. the overall resistance to dissolution).

In this work we investigate the dissolution behaviour of a set of P_2O_5-CaO-Na_2O glasses in deionised (DI) water and phosphate-buffered saline (PBS). In order to gain insight into the mechanisms of dissolution, we apply a two-stage model similar to that used by Ma et al. [22, 23] to describe the mass loss of Na-Fe-P and Na-Ca-P glasses, based on an initial parabolic time dependence, followed by later linear dissolution. To the authors' knowledge, this is the first work to quantitatively compare the non-linear mechanisms of P_2O_5-CaO-Na_2O glass dissolution in DI water and higher ionic strength PBS, across a range of pH values, and provides new insight into the two stages of dissolution, and the cause of the transition between them. The effect of pH is especially important when considering phosphate glasses as a component in polymer-glass composites, due to the acidification that can result from degradation of commonly used degradable polymers. To simulate the conditions phosphate glass may experience in a polymer-glass composite, we conducted dissolution experiments in PBS with added lactic acid (the acidic degradation product of common degradable polymers) to alter the solution pH, and determine the effect on the dissolution rate and mechanisms. Previous works have speculated that the transition between the two dissolution stages may be related to the nature of the conversion layer (also referred to as an alteration layer [23]), here we discuss how the formation of different conversion layer species across a range of solution conditions can affect the transition behaviour.

2. Materials and Methods

2.1. Glass preparation

Glasses with nominal compositions of $(P_2O_5)_{90\text{-}x}(CaO)_x(Na_2O)_{10}$, where x = 40, 45, 50, were prepared using Na_2CO_3, $CaCO_3$, and $NH_4H_2PO_4$, referred to subsequently by codes P50Ca40, P45Ca45, and P40Ca50 for x = 40, 45, 50 respectively. The precursors were melted and degassed in a kiln (SBSC-1500L, Kilns and Furnaces Ltd., Stoke-on-Trent, UK) at 1230 - 1360°C using a vitreous silica crucible, and then quenched quickly to room temperature. Glass discs (10 × 2 mm) were cast by pouring re-melted glass (at 1100 - 1230°C) into a graphite mould preheated to 400°C. Cast discs were then annealed at 400°C and left to cool slowly to room temperature, to remove any residual stresses.

2.2. Characterisation

Glass density was measured using an AccuPyc 1330 gas pycnometer (Micromeritics Instrument Corporation, USA). DSC (Differential scanning calorimetry) was carried out with a TA Instruments SDT Q600, using 10 - 25 mg of glass powder in an alumina pan, and heating from 25 to 1000°C at 20°C/min. Thermal properties were analysed using the TA Universal Analysis software. The data were baseline corrected by

subtracting the response of an empty alumina pan, and glass transition temperatures were taken at the inflection point. XRD (X-ray diffraction) was carried out using a Bruker D8 Advance diffractometer with Cu K-shell radiation. For confirming the amorphous nature of the disks, a 2θ range of 10-60˚with a 0.02˚step size and dwell time of 0.5 s/step was used, while a 2θ range of 20-50˚with a 0.1˚step size and dwell time of 10 s/step was used to maximise the signal/noise ratio for partially dissolved samples. SEM (Scanning electron microscopy) and EDX (Energy dispersive X-ray spectroscopy) were performed using a CamScan MX2600 FEG-SEM and Phenom ProX SEM, using an accelerating voltage of 10 kV for SEM and 15 kV for EDX. Prior to SEM/EDX, samples were sputter coated with approximately 10 nm of gold/palladium to prevent charging, using an Emitech K550 sputter coater (40 mA deposition current for 2 minutes, under an Argon atmosphere). The Q^n distribution in the glass network was measured by ^{31}P solid-state magic angle spinning (MAS) NMR, using a Bruker Avance 300 spectrometer at 121 MHz and a 4 mm MAS probe. 1D spectra were fitted using TopSpin 4.0.5 (Bruker Ltd.) to quantify the Q^n species present.

2.3. Dissolution testing

Dissolution tests were carried out in DI water (Type I, 18.2 MΩ) and PBS (phosphate-buffered saline, pH = 7) (Gibco, Thermo Fisher Scientific Inc., USA), as well as PBS adjusted to pH = 3, and pH = 5 by adding lactic acid (≥85%, Sigma-Aldrich 252476). Glass discs were immersed in 15 mL of the chosen solution (SA/V ratio 15 m^{-1}, chosen for comparison with published literature) in conical-bottomed vials (to ensure all surfaces were exposed to solution), and incubated at 37°C without agitation. Solution pH was measured using a Hanna HI 4222 pH meter with HI 1131B pH electrode and three point calibration. Ca^{2+} ion concentration was measured using an ISE (ion selective electrode - Sentek 361-75 Calcium Combination ISE), calibrated using a modified Nernst equation [25] with standard solutions diluted with DI water from a 0.1 mol L^{-1} calcium standard (Hanna HI 4004-01). To measure glass disc mass during dissolution, discs were removed from solution, rinsed with DI water, dabbed dry, and weighed (using a Sartorius BP61 balance with internal calibration, d = 0.1 mg), before being returned to the solution for further dissolution. Digital photographs were also taken to record visible changes in morphology. Before SEM imaging, partially dissolved discs were removed from solution, rinsed with DI water, dabbed dry, and stored in a desiccator to dry over several days.

3. Calculation

A two-stage dissolution model is used to describe the glass mass loss in a similar fashion to the work of Ma et al. [23], however here we adapt this model for use in a disc geometry by considering the thickness of a dissolved layer x. In the initial diffusion controlled stage (before the transition time t_{trans} is reached, i.e. $t < t_{trans}$), dissolution occurs at the surface of the disc and the interface moves towards the centre, resulting in the unreacted core shrinking and decreasing the surface and hence reaction area over time as shown in Fig. 1. In this stage a 3D diffusion model (DM) with parabolic time dependence applies [26, 27], such that:

$$x(t < t_{trans}) = k_{DM} t^{1/2} \tag{1}$$

In later stages ($t > t_{trans}$) the surface reaction determines the dissolution rate, with conversion reactions progressing into the disc by diffusion (as shown in Fig. 1), while dissolution of the conversion layer occurs at the surface. Assuming linear reaction kinetics the dissolution progress can be described by a contracting volume model [26, 28] (CVM):

$$x(t > t_{trans}) = k_{CVM} t \tag{2}$$

Therefore the extent of the dissolved layer over the whole course of dissolution can be described by:

$$x(t) = H(t_{trans} - t) k_{DM} t^{1/2} + H(t - t_{trans})(k_{DM} t_{trans}^{1/2} + k_{CVM}(t - t_{trans})) \tag{3}$$

where H is the Heaviside step function (half-maximum convention). Applying the disc geometry, the mass fraction dissolved (α) can be given by:

$$\alpha(t) = 1 - \frac{(r_0 - x(t))^2(h_0 - x(t))}{r_0^2 h_0} \tag{4}$$

where r_0 and h_0 are, respectively, the initial radius and height of the disc, as shown in Fig. 1. Equations 3 and 4 were used to model the mass loss of phosphate glasses, and were fitted to experimental data using non-linear least squares regression in Matlab.

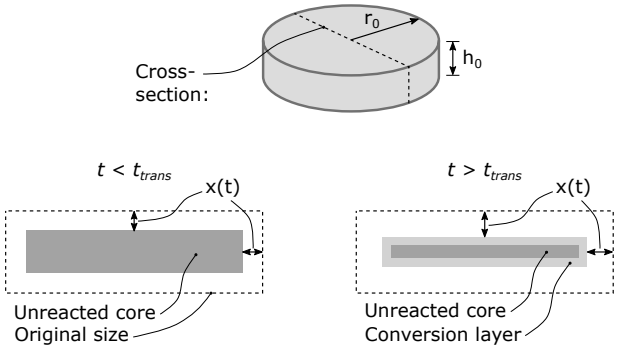

Figure 1: Schematic showing the model geometry for glass dissolution, and two-stage dissolution model as described by Eqs. 3 and 4.

4. Results

4.1. Characterisation

A summary of the properties of the prepared glass discs is shown in Table 1. The EDX-derived compositions indicated that the P_2O_5 and CaO content was consistent with that expected from the feed, however the Na_2O was lower than the 10 mol% expected, and the presence of SiO_2 (which was not included in the feed) was detected. O/P ratios are also given for comparison with other works. From ^{31}P MAS-NMR Q^1 and Q^2 phosphate tetrahedra (1 and 2 bridging oxygens respectively) were seen, at positions from -8.2 to -8.5 ppm for Q^1, and from -23.2 to -25.7 ppm for Q^2 [29–31]. As the Ca content increased the Q^1/Q^2 ratio increased, indicating depolymerisation of the network and replacement of chain forming Q^2 groups with chain terminating Q^1 groups. XRD did not detect the presence of any diffraction peaks, indicating that the glass discs used were completely amorphous.

Table 1: Measured physical and chemical properties of the glasses produced and used in this study. Compositions are measured by EDX, and the error shown is the standard deviation from measurements of three discs from the same batch.

Glass code	P_2O_5 (mol%)	CaO (mol%)	Na_2O (mol%)	SiO_2 (mol%)	O/P ratio	T_g (°C)	Q^1/Q^2	Density (g/cm^3)
P50Ca40	49.8 (±0.3)	40.1 (±0.3)	6.4 (±0.2)	3.7 (±0.2)	3.041 (±0.007)	451.6 (±0.7)	0.027 (±0.003)	2.6147 (±0.0009)
P45Ca45	44.8 (±0.3)	45.5 (±0.4)	6.9 (±0.2)	2.8 (±0.2)	3.147 (±0.009)	466.9 (±0.7)	0.36 (±0.02)	2.7062 (±0.0003)
P40Ca50	40.4 (±0.2)	50.8 (±0.4)	6.4 (±0.2)	2.4 (±0.2)	3.267 (±0.007)	489.5 (±0.5)	0.93 (±0.01)	2.784 (±0.001)

4.2. Dissolution in DI water

Solution pH and Ca^{2+} ion activity changes as the glasses dissolve in DI water are seen in Fig. 2. The control solution (DI water only) suffered a rapid decrease in pH to around 4.7 due to dissolution of atmospheric CO_2, followed by a gradual increase. This gradual increase can be attributed to contamination of the solution with residual ions from the electrode - in spite of thorough washing between samples, some transfer was unavoidable, and resulted in a pH increase for the control solution which has very low ionic concentration and therefore is very sensitive to changes.

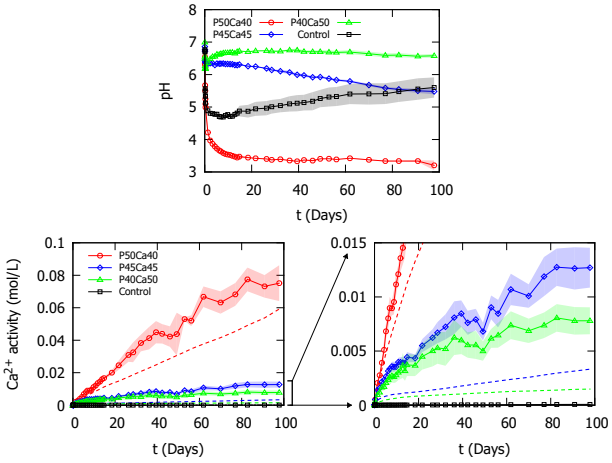

Figure 2: Solution pH (top) and Ca^{2+} activity (bottom) for phosphate glasses dissolving in DI water at 37°C. Solid lines indicate Ca^{2+} activity measured using an ISE, while dotted lines indicate Ca^{2+} activity calculated based on measured mass loss assuming congruent dissolution. Shaded region denotes standard deviation for n = 3 measurements.

Changes in measured Ca^{2+} ion activity indicate that the level of Ca released from the glass (Fig. 2) was the inverse of Ca content, with the lowest Ca glass (P50Ca40) releasing Ca the fastest - clearly Ca release is more closely linked to the dissolution behaviour (see below) than actual Ca content. Dotted lines in this graph indicate the Ca^{2+} activity calculated from the mass loss data (using the Truesdell-Jones model [32–34]) in Fig. 3, assuming congruent dissolution. In all cases the measured Ca release was significantly higher than that expected from the mass loss, indicating Ca was leached from the bulk glass.

The mass loss of phosphate glasses during dissolution in DI water (Fig. 3) shows that glasses with higher Ca content dissolved more slowly. It can also be seen that linear dissolution models (inset plots) did not describe this data adequately. By contrast the two-stage model, incorporating a diffusion stage (DM) and contracting volume stage (CVM), fitted the data well, with parameters given in Table S1 and Fig. 7. Rate constants (k_{DM}, k_{CVM}) decreased with increasing Ca, consistent with slower dissolution, while the transition time t_{trans} increased. The initial diffusion limited stage was not observed for the P50Ca40 glass, therefore t_{trans} can only be given as lower than the first non-zero timepoint.

The morphology of the phosphate glasses after dissolution in DI water is shown in Fig. 4. After 98 days a layer (denoted as type B) was observed on the surface of the P45Ca45 and P40Ca50 glasses. The morphology of this layer is difficult to interpret, as the cracks seen may be caused by the drying process, however the composition of this layer is of principal interest. EDX revealed this to be dominated by Ca and P, with a P:Ca:Na:Si ratio of 100:71:2:0 measured, regardless of the actual glass composition. A similar layer (B) with comparable composition was also seen partially covering the surface of the P50Ca40 glass, with the remaining area (denoted as type A) displaying etch pits. Areas where etch pits were found (only on P50Ca40) had a similar composition to the starting glass, however were depleted in Ca, with P:Ca:Na:Si ratio of 100:33:15:4, compared with a ratio of 100:40:13:4 before dissolution. This layer was also seen in

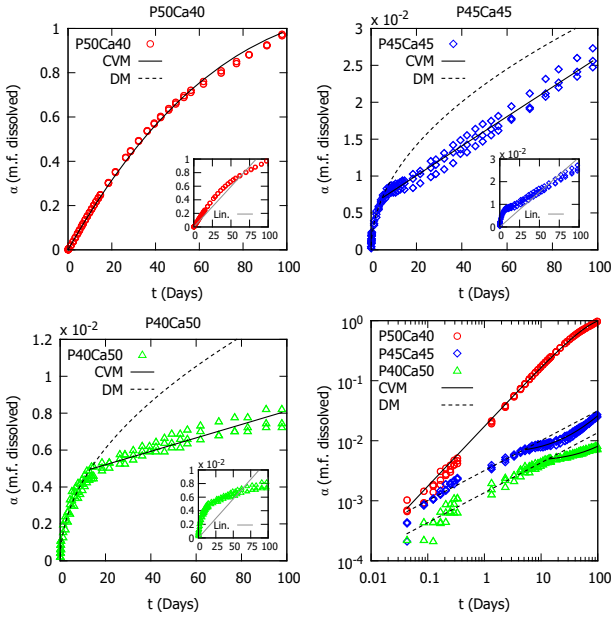

Figure 3: Mass fraction dissolved during dissolution in DI water at 37°C for phosphate glasses, fitted to two-stage model with diffusion stage (dotted line - DM) and contracting volume stage (solid line - CVM). Inset plots show the same data fitted to a linear dissolution rate. Bottom right shows the same data combined onto a log-log scale for comparison.

macro-scale images of the glass discs, where it turned the transparent glass opaque (Fig. 4). The time at which this layer appeared roughly corresponded to the transition time between the two stages of mass loss (Table S1) for the medium and high Ca glass (P45Ca45 and P40Ca50), however for the low Ca glass P50Ca40 transition occurred very early on, while the layer was only visible well into the dissolution process. The appearance of the glass discs shown in Fig. 4e is consistent with the assumption of homogeneous size reduction inherent in this model. When dissolution is nearly complete, this assumption would predict a very thin disc with slightly reduced diameter, which is consistent with the appearance of the P50Ca40 disc after 98 days in DI water (mass fraction dissolved $\alpha = 0.97$). The hole that has appeared in the disc is a result of slight variations in disc thickness across the surface (on the scale of tens of microns) leading to complete dissolution in some places but not others.

4.3. Dissolution in PBS

The evolution of solution pH during phosphate glass dissolution in PBS and pH-adjusted PBS is shown in Fig. 5. The trend for different glass compositions is consistent with dissolution in DI water (Fig. 2), with higher Ca glasses leading to higher solution pH. In general, regardless of initial pH, the dissolution of the glass in PBS appeared to result in a slow convergence of the solution pH towards a similar value for each glass composition as the glass dissolution slowly dominated over the initial solution conditions. The pH of the empty solution (PBS) was measured to be stable at pH ≈ 7 over the experimental timescale used.

The mass loss of phosphate glasses in PBS and pH-adjusted PBS is shown in Fig. 6, with fitted curves from the two-stage model in Table S1. Again it is clear that glasses with higher Ca content dissolved more slowly, in accordance with earlier results in DI water. The effect of pH on the general mass loss trend is also clear; reduced pH accelerated mass loss for all glass compositions.

The fitted parameters for the two-stage model (Table S1 and Fig. 7) showed significant variation across glass composition and solution conditions. The rate constant for the diffusion controlled stage (k_{DM}) showed

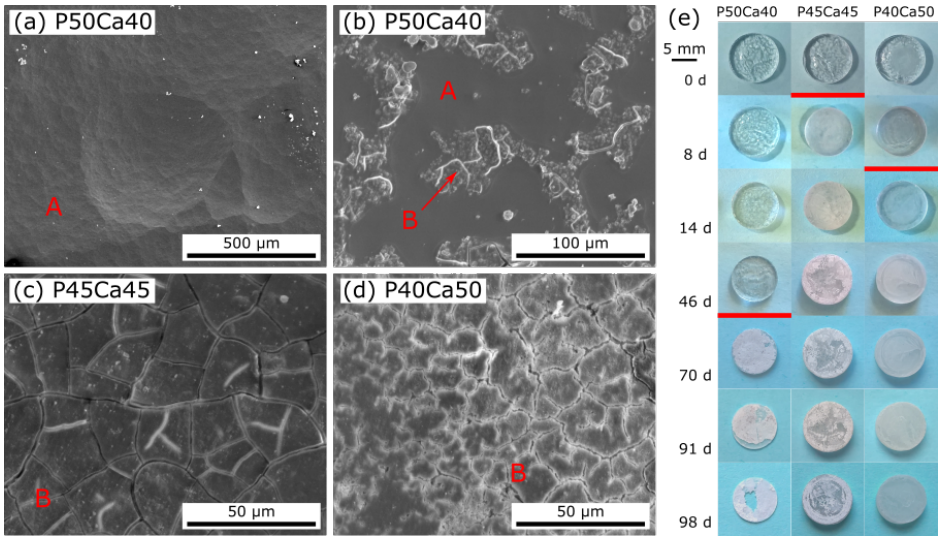

Figure 4: Morphology of glass discs during and after dissolution, showing SEM images after 98 days in DI water at 37°C for P50Ca40 (a, b), P45Ca45 (c), P40Ca50 (d), and digital photographs of glass discs at various dissolution timepoints (e). Red lines indicate the time taken for observation of an opaque layer.

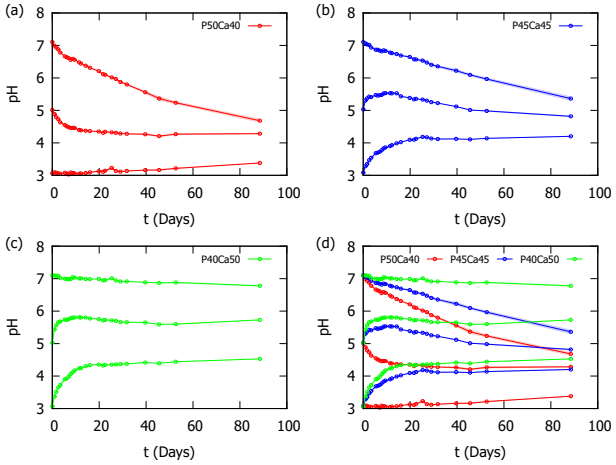

Figure 5: Solution pH for phosphate glasses dissolving in PBS, or lactic acid-adjusted PBS at pH 3 or 5, at 37°C, showing P50Ca40 (a), P45Ca45 (b), P40Ca50 (c), and all three glasses together for comparison (d). Shaded region denotes standard deviation for n = 3 measurements.

a clear decreasing trend for increasing Ca content, and also increased significantly as the solution pH decreased. Similar trends, although less clear, were also seen for the rate constant for the reaction controlled stage (k_{CVM}). Variation in the transition time (t_{trans}) between the two stages was also seen across different glass compositions and solution conditions. In DI water, t_{trans} increased with increasing Ca content, however this trend was absent in PBS with a similar t_{trans} observed for all glass compositions, and reversed in pH-adjusted PBS, with a decreasing t_{trans} with increasing Ca content.

The macro-scale morphology of glass discs during dissolution is shown in Fig. 8, where the formation of an opaque layer was observed for all glasses except for P50Ca40 in pH 3 and pH 5. The time taken for observation of this layer is also shown plotted against the fitted t_{trans} parameter in Fig. 9. Data points for P50Ca40 in DI water and PBS at pH 3 and 5 were excluded from this plot as transition occurred immediately

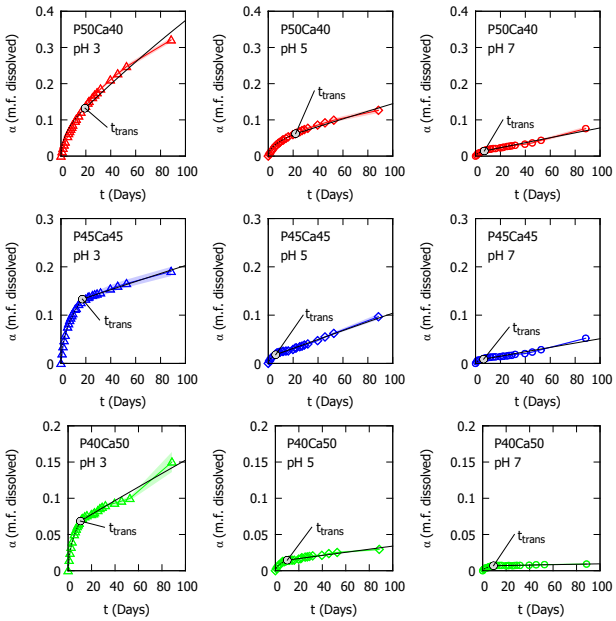

Figure 6: Mass fraction dissolved during dissolution in PBS, or lactic acid-adjusted PBS at pH 3 or 5, at 37°C. Shaded region denotes standard deviation for n = 3 measurements. Black line shows fitted model according to Eq. 4, with dotted and solid regions denoting the diffusion and contracting volume stages respectively.

in DI water, and no layer was observed in PBS at pH 3 and 5 within the duration of the experiment.Good correlation can be observed between these two values, giving a Pearson correlation coefficient (r) of 0.7. A more detailed view of the morphology is shown by SEM analysis in Fig. 10, where several types of dissolution behaviour can be seen.

Type A dissolution (Fig. 10a) consisted of etch pits in the glass surface, and was seen by EDX to be depleted in Ca compared with the original glass. Type A dissolution was observed at dissolution times below t_{trans}, as well as at the end of the study (88 days) for P50Ca40 glass in pH 3 or 5. Type B dissolution (Fig. 10c-f) consisted of formation of a layer rich in Ca but also K, and depleted in Na. This layer was be identified by EDX but could not be detected by XRD (Fig. 11), suggesting that the layer had very little long-range crystalline order [18]. The presence of K in this layer was attributed to the PBS used, the original glasses did not contain any, however the solution was rich in potassium. The cross section shown in Fig. 10 revealed some information about the morphology of this layer, where a dense initial portion was seen, below a more porous section. Fig. 10f is also interesting to note, as the remnants of type A etch pits (lighter lines across the surface) were visible below the more porous type B layer. Type C dissolution (Fig. 10b) consisted of formation of a NaCl layer on the glass surface, which could be identified by EDX and XRD (Fig. 11). This NaCl layer was only observed at dissolution times slightly above t_{trans}, but not at the end of the study (88 days).

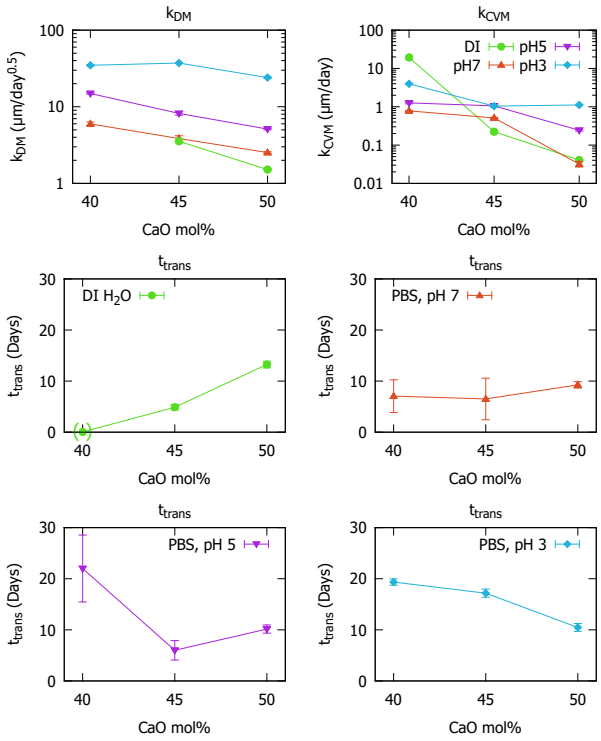

Figure 7: Fitted parameters (k_{DM}, k_{CVM}, t_{trans}) for the two-stage model for phosphate glass dissolution in DI water, PBS, or lactic acid-adjusted PBS at pH 3 or 5, at 37°C C. Error bars denote standard deviation for n = 3 measurements, brackets () denote transition occurring immediately, with no diffusion-limited stage observed.

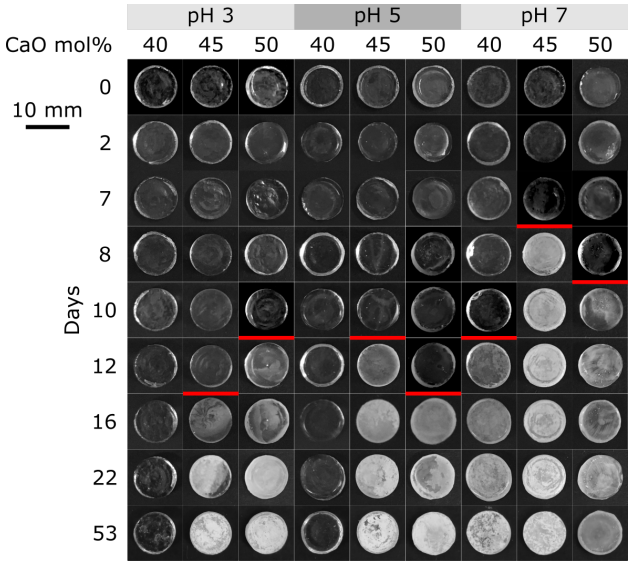

Figure 8: Morphology of glass discs during and after dissolution in PBS, or lactic acid-adjusted PBS at pH 3 or 5, at 37°C. Red lines indicate the time taken for observation of an opaque layer.

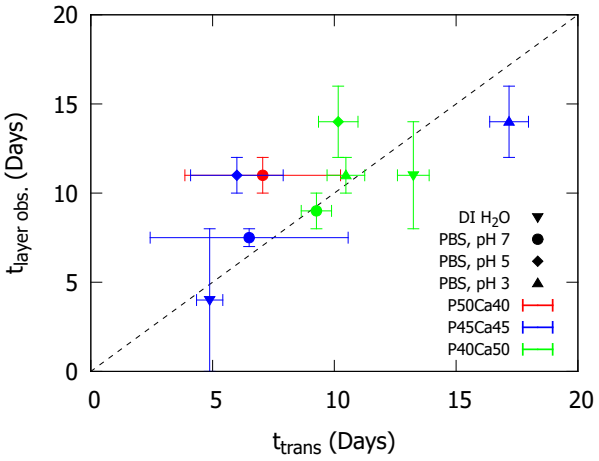

Figure 9: Comparison of fitted t_{trans} parameter, and the time taken to observe formation of an opaque layer on the glass surface. Colours denote glass compositions, and symbols denote the dissolution media, as described in the key. Dotted line represents $t_{trans} = t_{layer\ obs}$.

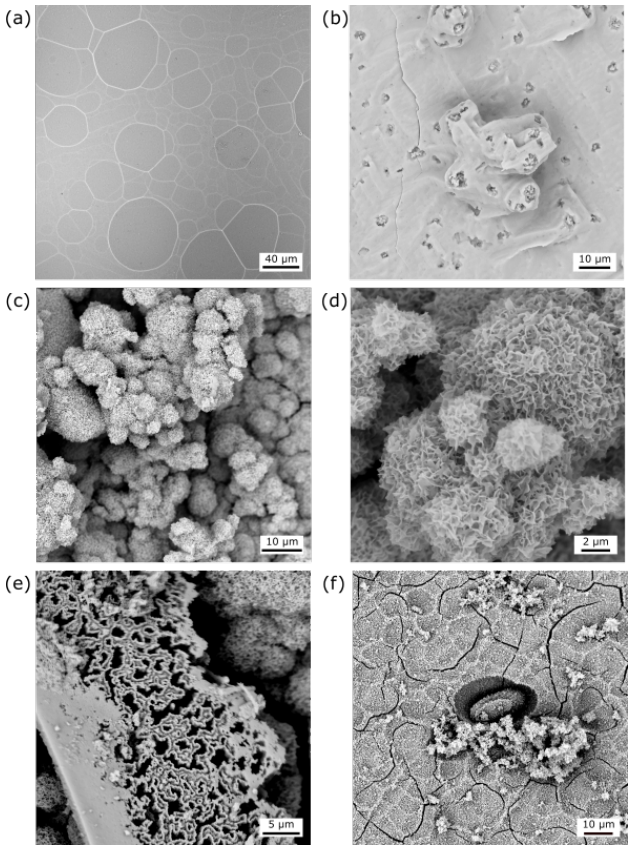

Figure 10: SEM images of phosphate glasses during dissolution showing (a) type A behaviour (etch pits) on P45Ca45 in pH 3 below t_{trans}, and (b) type C behaviour (NaCl layer formation) on P40Ca50 in pH 7 above t_{trans}. (c-f) show type B behaviour (CaP layer formation): on P45Ca45 in pH 3 after 88 days (c, d), on P40Ca50 in pH 3 after 88 days (e), and on P40Ca50 in pH 7 above t_{trans} (f).

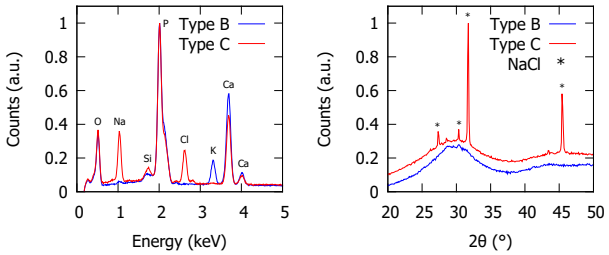

Figure 11: EDX spectra (left), and XRD patterns (right), for representative samples displaying type B (CaP layer formation) and type C (NaCl layer formation) behaviour. XRD patterns are offset vertically for clarity.

5. Discussion

5.1. Structure

The replacement of Na_2O by SiO_2 can be attributed to volatilisation of Na from the melt, and replacement by Si from the silica crucible [35]. The results observed for characterisation of the phosphate glasses produced (Table 1) were consistent with a modified version of the nominal glass model, incorporating the presence of SiO_2 from the crucible: $(P_2O_5)_{90\text{-}x}(CaO)_x(Na_2O)_7(SiO_2)_3$. Here the network of phosphate tetrahedra was depolymerised by the addition of other metal ions, which created non-bridging oxygens according to their charge, resulting in the Q^1/Q^2 ratios observed. The increase in density with Ca content was consistent with Ca ions being located at interstitial sites within the phosphate network, forming crosslinks between phosphate glass chains [6, 17]. The effect of these crosslinks was seen in the increased T_g for higher Ca glasses - Ca crosslinks provided greater thermal resistance so increase the T_g [6, 36]. These crosslinks are also known to provide greater chemical durability, so would be expected to lead to a slower dissolution rate.

The presence of small amounts of SiO_2 in phosphate glasses such as the amount observed in this study are known to disrupt the phosphate glass network, which in turn leads to a slight increase in the glass dissolution rate [37]. This indicates that the presence of this impurity may have increased the glass dissolution rate above that which would be expected without these impurities. With the glasses used here, the SiO_2 content is relatively consistent across the glass compositions at around 3 mol. %, so this is unlikely to make a significant contribution to the trends observed. Formation of six-fold coordinated Si ions, which can reduce the dissolution rate, has been previously observed in phosphate glasses. However, this requires a higher degree of network connectivity within the phosphate glass network (mostly Q^3 phosphates) than is present here (only Q^2 or Q^1), as well as a greater concentration of Si, so their presence is not expected in these glass compositions [38, 39]. Formation of six-fold coordinated Si ions would also result in the appearance of a unique peak at 670 cm^{-1} in the IR spectrum [38], which was not observed in our experiments (Fig. S4).

5.2. Dissolution kinetics

Although phosphate glasses have been researched for several decades now, the mechanisms of their dissolution are still a source of uncertainty [22], and it is hoped that the results described here can provide some additional insight into these mechanisms. Here we propose the following explanation for the observed dissolution behaviour, which can be broadly broken down into two main categories of reaction. Firstly we introduce the idea of the formation of a conversion layer, which can include hydration among other reactions. Secondly, layer dissolution reactions encompass dissolution of the various products of conversion layer formation, involving release of ions into solution. It must be noted that both of these reaction categories take place simultaneously throughout the dissolution process, however at various points one or other of these may be rate-limiting. A summary of this mechanism scheme is shown in Fig. 12.

Conversion layer formation involves reaction of crosslinked phosphate glass anions in the solid state, with reactants that have diffused into the glass such as H_2O, H^+ and Cl^-. This results in formation of other solid species, usually including the hydration reaction to form hydroxides, but possibly other reactions as well. The hydration reaction (Eq. 5) has been described by Ma et al. [22], defining the hydration of crosslinks between metal cations and two phosphate anions (with n and m phosphate tetrahedra). This is adequate for dissolution in DI water, however the situation is more complex for solutions such as PBS where various other ions are present in solution. Formation of metal hydroxides can be replaced by, or occur in conjunction with, reactions to form solid metal chlorides as described in Eq. 6. This is particularly significant given the much greater solubility in water of $CaCl_2$ compared with $Ca(OH)_2$.

$$(P_nO_{3n+1})(Ca,Na_2)_{(n+m+4)/2}(P_mO_{3m+1}) + (n+m+4)H_2O \rightarrow H_{2+n}P_nO_{3n+1} + H_{2+m}P_mO_{3m+1} + (n+m+4)/2(Ca,Na_2)(OH)_2 \quad (5)$$

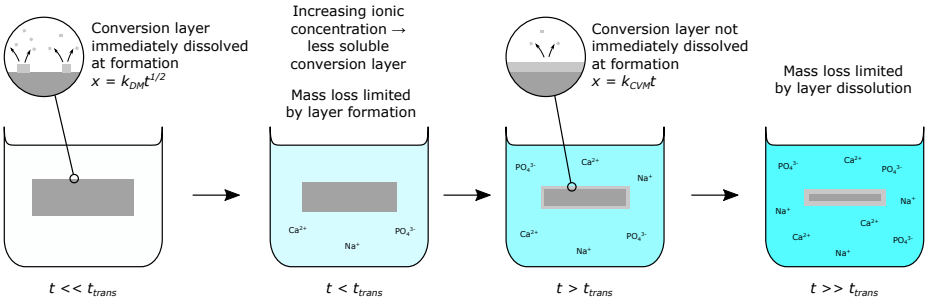

Figure 12: Schematic diagram illustrating dissolution mechanism, showing diffusion limited dissolution before t_{trans}, and surface reaction limited dissolution after t_{trans} when the conversion layer is stable.

$$(P_nO_{3n+1})(Ca,Na_2)_{(n+m+4)/2}(P_mO_{3m+1}) + (n+m+4)H^+ + (n+m+4)Cl^- \rightarrow H_{2+n}P_nO_{3n+1} + H_{2+m}P_mO_{3m+1} + (n+m+4)/2(Ca,Na_2)Cl_2 \quad (6)$$

The reaction front for these conversion layer formation reactions progresses into the glass, following a parabolic time dependence ($t^{1/2}$) due to the diffusive mass transport required to transport reactants to the reaction front. This is supported by the observed formation of a NaCl layer during dissolution, as well as Ca-rich layers (Figs. 10 and 11).

Layer dissolution is the second reaction stage, involving surface dissolution of the solid species formed during the conversion layer formation stage, described in Eqs. 7-9. As shown in Eq. 9, orthophosphoric acid (n=1) can dissolve directly, while polyphosphates can undergo further hydrolysis. Nevertheless, it is well known that polyphosphates can be released into solution without further hydrolysis [22, 40].

$$(Ca,Na_2)(OH)_2 \rightarrow (Ca,Na_2)^{2+} + 2OH^- \quad (7)$$

$$(Ca,Na_2)Cl_2 \rightarrow (Ca,Na_2)^{2+} + 2Cl^- \quad (8)$$

$$H_{2+n}P_nO_{3n+1} + (n-1)H_2O \rightarrow (3n)H^+ + nPO_4^{3-} \quad (9)$$

The reaction front for these layer dissolution reactions progresses into the conversion layer, following a linear time dependence (t) due to the reaction controlled process. The dissolution of solid species via these reactions will be sensitive to solution conditions, not only pH but various ion concentrations, which can themselves change over time as the glass dissolves. Depending on ion concentrations, reverse reactions can also occur in a highly saturated solution, involving reaction of solution ions to form a precipitate on the glass surface. This is especially important for metal phosphates, as shown in Eq. 10, where metal and phosphate ions (resulting from glass dissolution, or already present in PBS) form metal phosphates. Eq. 10 shows formation of simple phosphates, but more complex forms such as octacalcium phosphate or hydroxyapatite are also possible, as suggested by the morphology of the Ca-rich layer observed (Figs. 10 and 11) [18, 41].

$$3(Ca,Na_2,K_2)^{2+} + 2PO_4^{3-} \rightarrow (Ca,Na_2,K_2)_3(PO_4)_2 \quad (10)$$

These two reaction categories can explain the multi-stage dissolution behaviour observed here and elsewhere. Initially the conversion layer formation reactions, which must occur first to produce soluble salts, are rate-limiting due to fast dissolution of the small amounts of hydrated phosphates and metal hydroxides or chlorides produced. As this reaction is limited by mass transport of reactants to the reaction front, this

leads to the initial $t^{1/2}$ dependence of the reaction progress x. As the conversion layer dissolves as fast as it is formed, there is no stable conversion layer present on the surface. In later stages ($t > t_{trans}$) the layer dissolution reactions determine the glass dissolution rate, giving rise to the linear t dependence due to assumed linear reaction kinetics. Here the conversion layer is produced faster than it can be dissolved, leading to buildup of the layer on the surface, as illustrated in Fig. 1. Despite encompassing dissolution of several layer species (Eqs. 7-9), as well as deposition reactions (Eq. 10), glass dissolution controlled by dissolution of the conversion layer can be adequately described by Eq. 2 of the model. Assuming Eqs. 7-10 proceed via linear reaction kinetics, k_{CVM} is simply the sum of equivalent parameters for individual reactions. k for deposition reactions will be negative, and if deposition outweighs mass loss, k_{CVM} will be negative, leading to overall mass gain.

The effect of Ca on the dissolution rate in the initial conversion layer formation stage seen here is consistent with multiple previous works, where increased Ca content reduced the dissolution rate [7, 8, 36]. Higher Ca glasses were shown to have higher density (Table 1), indicating that Ca ions were located at interstitial sites between phosphate glass chains, reducing the free volume [35]. In this diffusion controlled stage, this resulted in reduced dissolution (lower k_{DM}) by blocking of interstitial diffusion pathways. The greater strength of the Ca-O-P crosslinks compared with P-O-P bonds is another reason for the reduced dissolution rate of higher Ca glasses [15]. The rate constant governing this diffusion stage (k_{DM}) was shown to have a significant dependence on the starting solution pH (Fig. 7), with large increases in k_{DM} observed as the pH of the solution was reduced. This is consistent with a diffusion mechanism involving H^+ diffusion into the glass, which would be increased by a larger H^+ concentration in the solution.

The later stages of dissolution are limited by the surface reactions (Eqs. 7-10), leading to the formation of a stable conversion layer, which persists as it is formed faster than it dissolves. The effect of Ca on the reaction rate here also displays reduced dissolution with increasing Ca content. This can be explained in terms of the hydration reaction (Eq. 5), which indicates that production of the less soluble $Ca(OH)_2$ would dominate over NaOH as the Ca/Na ratio increases. Similarly, when PO_4^{3-} concentration is sufficient, precipitation of phosphates according to Eq. 10 would prefer less soluble calcium phosphates, further reducing the mass loss. The effect of pH in this layer dissolution stage is complex, however in general lower pH increases the reaction rate constant k_{CVM}, which can be attributed to increased solubility of the conversion layer species in more acidic conditions.

The transition time between these two stages is perhaps the least well understood component of the non-linear dissolution of phosphate glasses. Bunker et al. described a rough correlation between glass durability and transition time, also noting that it was also sensitive to pH [15], while Ma et al. found that the transition time only varied for glasses with short phosphate chains (i.e. higher O/P and Q^1/Q^2 ratios), finding a similar correlation to Bunker et al., but also commenting that it may be related to the nature of the surface layer [23]. In this work we observed a similar correlation to Bunker et al. for dissolution in DI water (more soluble glasses have a shorter transition time), however this trend was absent in PBS and was reversed in pH-adjusted PBS (pH = 3 or 5).

Under the mechanism proposed here, the transition from the conversion layer formation stage to the layer dissolution stage is controlled predominantly by the nature of the conversion layer (i.e. the combination of solid species formed by Eqs. 5-6) and its solubility in the surrounding solution, which will be heavily dependent on pH and ion concentrations. As the solution chemistry changes during dissolution, increases in dissolved metal (Ca, Na), hydroxide, and phosphate ions will reduce the dissolution rate of the conversion layer. Once the dissolution rate is lower than the formation rate, the conversion layer is stabilised, and the rate limiting reaction will become the layer dissolution, leading to a change from parabolic ($t^{1/2}$) to linear (t) reaction kinetics. When this stable layer is dominated by $(Ca,Na_2)(OH)_2$ or $(Ca,Na_2)Cl_2$, or deposited phosphates (Eq. 10), it would be expected to be optically opaque as observed in Fig. 8, explaining the correlation between t_{trans} and the time for observation of an opaque layer (Fig. 9). The behaviour of P50Ca40 glass seemed to contradict this however, displaying transition to the linear layer dissolution kinetics in DI

water, and PBS at pH 3 or 5, without formation of an opaque layer. This can be explained by differences in the phosphate anions present. Based on the glass composition, the number average chain length can be calculated [15]; for P50Ca40, P45Ca45, and P40Ca50 the average chain length (n) is predicted to be ∞, 9.1 and 4.0 respectively. This means that in acidic conditions, layer dissolution from P50Ca40 may be limited by the hydrolysis reaction of longer phosphate chains (Eq. 9, where n is very large) rather than dissolution of other solid species. Transition to this stage would then not result in a visible opaque layer, as the hydrated phosphate anions ($H_{2+n}P_nO_{3n+1}$) that make up the conversion layer are not forming a new crystalline solid but rather their cation crosslinkers are simply being exchanged for H^+ ions.

6. Conclusions

These results offer new insight into the mechanism of phosphate glass dissolution in various media, in particular the origin of the parabolic time dependence and transition time between the two stages. Understanding the dissolution behaviour of these glasses is of importance when considering their dissolution in medical applications, and the pH dependence of this is particularly of interest in polymer composite applications, where polymer degradation results in formation of lactic acid and acidification.

The dissolution behaviour of a range of P_2O_5-CaO-Na_2O glasses was measured in deionised water, PBS, and pH-adjusted PBS at pH 3 or 5. In accordance with previous studies in DI water, increased Ca was observed to significantly reduce the dissolution rate in all conditions. Two-stage behaviour was seen in DI water, PBS, and pH-adjusted PBS, with an initial parabolic time dependence, followed by later linear time dependent reaction progression. A two-stage model similar to those reported previously was adapted for use with the disc-shaped glass samples here.

Based on these results, a new dissolution mechanism was proposed to explain the two-stage dissolution behaviour, that takes into account more complex dissolution media. The initial stage involves diffusion of water or ions into the glass, with $t^{1/2}$ dependence, forming a conversion layer consisting of hydrated phosphate anions, and metal hydroxides or chlorides. Once the solution conditions slow the layer dissolution reactions enough so that the conversion layer is stabilised, the layer dissolution reaction becomes rate-limiting and results in linear t dependence. Under this mechanism, the transition time t_{trans} is sensitive both to the nature of the conversion layer, and the solution conditions.

Acknowledgements

The authors thank Lucideon Ltd. for financial support of the project, and for providing facilities for production of phosphate glass materials. In particular, the assistance of Mr Ian Campbell is greatly appreciated. We would also like to thank Dr Abil Aliev at University College London, for collecting the solid-state NMR spectra. RNO would also like to thank the Woolf Fisher Trust and the Cambridge Trust, for provision of a PhD scholarship, and the Armourers and Brasiers' Company for additional funding. The authors would also like to thank Dr Kyung-Ah Kwon, Mr Wayne Skelton-Hough, Dr Christopher Lovell, Mr Simon Griggs, and Mr Robert Cornell for their technical support and helpful discussions throughout the project. Original data for this paper can be found at https://doi.org/10.17863/CAM.50847.

References

[1] S. Kargozar, F. Baino, S. Hamzehlou, R. G. Hill, and M. Mozafari, "Bioactive Glasses: Sprouting Angiogenesis in Tissue Engineering," *Trends in Biotechnology*, vol. 36, no. 4, pp. 430–444, 2018.

[2] M. Bitar, V. Salih, V. Mudera, J. C. Knowles, and M. P. Lewis, "Soluble phosphate glasses: in vitro studies using human cells of hard and soft tissue origin," *Biomaterials*, vol. 25, no. 12, pp. 2283–2292, 2004.

[3] A. R. Boccaccini, D. S. Brauer, and L. Hupa, eds., *Bioactive Glasses*. Smart Materials Series, Cambridge: Royal Society of Chemistry, 2016.
[4] R. Shah, A. Sinanan, J. Knowles, N. Hunt, and M. Lewis, "Craniofacial muscle engineering using a 3-dimensional phosphate glass fibre construct," *Biomaterials*, vol. 26, no. 13, pp. 1497–1505, 2005.
[5] E. Abou Neel, I. Ahmed, J. Pratten, S. Nazhat, and J. Knowles, "Characterisation of antibacterial copper releasing degradable phosphate glass fibres," *Biomaterials*, vol. 26, no. 15, pp. 2247–2254, 2005.
[6] A. Parsons, L. Burling, C. Scotchford, G. Walker, and C. Rudd, "Properties of sodium-based ternary phosphate glasses produced from readily available phosphate salts," *Journal of Non-Crystalline Solids*, vol. 352, no. 50, pp. 5309–5317, 2006.
[7] J. C. Knowles, "Phosphate based glasses for biomedical applications," *Journal of Materials Chemistry*, vol. 13, no. 10, p. 2395, 2003.
[8] E. A. Abou Neel, D. M. Pickup, S. P. Valappil, R. J. Newport, and J. C. Knowles, "Bioactive functional materials: a perspective on phosphate-based glasses," *Journal of Materials Chemistry*, vol. 19, no. 6, pp. 690–701, 2009.
[9] N. Sharmin, M. S. Hasan, A. J. Parsons, C. D. Rudd, and I. Ahmed, "Cytocompatibility, mechanical and dissolution properties of high strength boron and iron oxide phosphate glass fibre reinforced bioresorbable composites," *Journal of the Mechanical Behavior of Biomedical Materials*, vol. 59, pp. 41–56, 2016.
[10] R. Felfel, I. Ahmed, A. Parsons, G. Palmer, V. Sottile, and C. Rudd, "Cytocompatibility, degradation, mechanical property retention and ion release profiles for phosphate glass fibre reinforced composite rods," *Materials Science and Engineering: C*, vol. 33, no. 4, pp. 1914–1924, 2013.
[11] M. Shah Mohammadi, I. Ahmed, N. Muja, C. D. Rudd, M. N. Bureau, and S. N. Nazhat, "Effect of phosphate-based glass fibre surface properties on thermally produced poly(lactic acid) matrix composites," *Journal of Materials Science: Materials in Medicine*, vol. 22, no. 12, pp. 2659–2672, 2011.
[12] J. E. Gough, P. Christian, C. A. Scotchford, C. D. Rudd, and I. A. Jones, "Synthesis, degradation, and in vitro cell responses of sodium phosphate glasses for craniofacial bone repair," *Journal of Biomedical Materials Research*, vol. 59, no. 3, pp. 481–489, 2002.
[13] J. E. Gough, P. Christian, C. A. Scotchford, and I. A. Jones, "Long-term craniofacial osteoblast culture on a sodium phosphate and a calcium/sodium phosphate glass," *Journal of Biomedical Materials Research*, vol. 66A, no. 2, pp. 233–240, 2003.
[14] A. J. Parsons, M. Evans, C. D. Rudd, and C. A. Scotchford, "Synthesis and degradation of sodium iron phosphate glasses and their in vitro cell response," *Journal of Biomedical Materials Research - Part A*, vol. 71, no. 2, pp. 283–291, 2004.
[15] B. Bunker, G. Arnold, and J. Wilder, "Phosphate glass dissolution in aqueous solutions," *Journal of Non-Crystalline Solids*, vol. 64, no. 3, pp. 291–316, 1984.
[16] M. Uo, M. Mizuno, Y. Kuboki, A. Makishima, and F. Watari, "Properties and cytotoxicity of water soluble Na2O–CaO–P2O5 glasses," *Biomaterials*, vol. 19, no. 24, pp. 2277–2284, 1998.
[17] J. R. Van Wazer and D. A. Campanella, "Structure and Properties of the Condensed Phosphates. IV. Complex Ion Formation in Polyphosphate Solutions," *Journal of the American Chemical Society*, vol. 72, no. 2, pp. 655–663, 1950.
[18] K. Franks, I. Abrahams, and J. C. Knowles, "Development of soluble glasses for biomedical use Part I: In vitro solubility measurement," *Journal of Materials Science: Materials in Medicine*, vol. 11, no. 10, pp. 609–614, 2000.
[19] V. Salih, K. Franks, M. James, G. W. Hastings, J. C. Knowles, and I. Olsen, "Development of soluble glasses for biomedical use Part II: The biological response of human osteoblast cell lines to phosphate-based soluble glasses," *Journal of Materials Science: Materials in Medicine*, vol. 11, no. 10, pp. 615–620, 2000.
[20] J. Massera, K. Bourhis, L. Petit, M. Couzi, L. Hupa, M. Hupa, J. Videau, and T. Cardinal, "Effect of the glass composition on the chemical durability of zinc-phosphate-based glasses in aqueous solutions," *Journal of Physics and Chemistry of Solids*, vol. 74, no. 1, pp. 121–127, 2013.
[21] F. Delahaye, L. Montagne, G. Palavit, J. Claude Touray, and P. Baillif, "Acid dissolution of sodium-calcium metaphosphate glasses," *Journal of Non-Crystalline Solids*, vol. 242, no. 1, pp. 25–32, 1998.
[22] L. Ma, R. K. Brow, and M. E. Schlesinger, "Dissolution behaviour of sodium calcium polyphosphate glasses," *Physics and Chemistry of Glasses: European Journal of Glass Science and Technology Part B*, vol. 59, no. 5, pp. 205–212, 2018.
[23] L. Ma, R. K. Brow, and M. E. Schlesinger, "Dissolution behavior of Na2O-FeO-Fe2O3-P2O5 glasses," *Journal of Non-Crystalline Solids*, vol. 463, pp. 90–101, 2017.
[24] N. Sharmin and C. D. Rudd, "Structure, thermal properties, dissolution behaviour and biomedical applications of phosphate glasses and fibres: a review," *Journal of Materials Science*, vol. 52, no. 15, pp. 8733–8760, 2017.
[25] D. Midgley, "The interpretation of non-ideal calibrations of ion-selective electrodes," *Analytical Chemistry*, vol. 49, no. 8, pp. 1211–1218, 1977.
[26] M. N. Rahaman, *Ceramic processing and sintering*. New York: Marcel Dekker Inc., 2 ed., 2003.
[27] Y. Gu, W. Xiao, L. Lu, W. Huang, M. N. Rahaman, and D. Wang, "Kinetics and mechanisms of converting bioactive borate glasses to hydroxyapatite in aqueous phosphate solution," *Journal of Materials Science*, vol. 46, no. 1, pp. 47–54, 2011.
[28] S. B. Jung and D. E. Day, "Conversion kinetics of silicate, borosilicate, and borate bioactive glasses to hydroxyapatite," *Physics and Chemistry of Glasses - European Journal of Glass Science and Technology Part B*, vol. 50, no. 2, pp. 85–88, 2009.
[29] R. K. Brow, "Review: the structure of simple phosphate glasses," *Journal of Non-Crystalline Solids*, vol. 263, pp. 1–28, 2000.
[30] J. P. Fletcher, R. J. Kirkpatrick, D. Howell, and S. H. Risbud, "31P Magic-angle spinning nuclear magnetic resonance spectroscopy of calcium phosphate glasses," *Journal of the Chemical Society, Faraday Transactions*, vol. 89, no. 17, p. 3297, 1993.

[31] P. Gras, A. Baker, C. Combes, C. Rey, S. Sarda, A. J. Wright, M. E. Smith, J. V. Hanna, C. Gervais, D. Laurencin, and C. Bonhomme, "From crystalline to amorphous calcium pyrophosphates: A solid state Nuclear Magnetic Resonance perspective," *Acta Biomaterialia*, vol. 31, pp. 348–357, 2016.
[32] A. H. Truesdell and B. F. Jones, "WATEQ, a computer program for calculating chemical equilibria of natural waters," *Journal of the U.S. Geological Survey*, vol. 2, no. 2, pp. 233–248, 1974.
[33] R. M. Garrels and C. L. Christ, *Solutions, minerals, and equilibria*. New York: Harper & Row, 1965.
[34] J. I. Drever, *The Geochemistry of Natural Waters*. Englewood Cliffs, N.J.: Prentic-Hall Inc., 1982.
[35] J. E. Shelby, *Introduction to glass science and technology*. Royal Society of Chemistry, 2005.
[36] I. Ahmed, M. Lewis, I. Olsen, and J. Knowles, "Phosphate glasses for tissue engineering: Part 1. Processing and characterisation of a ternary-based P2O5–CaO–Na2O glass system," *Biomaterials*, vol. 25, no. 3, pp. 491–499, 2004.
[37] A. Patel and J. C. Knowles, "Investigation of silica-iron-phosphate glasses for tissue engineering," *Journal of Materials Science: Materials in Medicine*, vol. 17, pp. 937–944, 2006.
[38] H. Tabuchi, N. Kuriyama, and S. Morimoto, "Effects of SiO2 Substitution on the Structure and Properties of Low-Melting Phosphate Glass," *Journal of the Ceramic Society of Japan*, vol. 102, no. 3, pp. 221–224, 1994.
[39] J. Ren and H. Eckert, "Superstructural Units Involving Six-Coordinated Silicon in Sodium Phosphosilicate Glasses Detected by Solid-State NMR Spectroscopy," *Journal of Physical Chemistry C*, vol. 122, pp. 27620–27630, 2018.
[40] E. A. Abou Neel, W. Chrzanowski, and J. C. Knowles, "Effect of increasing titanium dioxide content on bulk and surface properties of phosphate-based glasses," *Acta Biomaterialia*, vol. 4, no. 3, pp. 523–534, 2008.
[41] F. Barrère, C. M. van der Valk, R. A. J. Dalmeijer, C. A. van Blitterswijk, K. de Groot, and P. Layrolle, "In vitro and in vivo degradation of biomimetic octacalcium phosphate and carbonate apatite coatings on titanium implants," *Journal of Biomedical Materials Research Part A*, vol. 64A, no. 2, pp. 378–387, 2003.

Supplementary Material: Non-linear dissolution mechanisms of P_2O_5-CaO-Na_2O glasses as a function of pH in various aqueous media

Reece N. Oosterbeek, Kalliope I. Margaronis, Xiang C. Zhang, Serena M. Best, Ruth E. Cameron

S.1. Glass characterisation

XRD patterns for the phosphate glasses used are shown in Figs. S1 and S2. After initial quenching the P40Ca50 glass showed a small amount of devitrification due to the high amount of modifiers present, as indicated by the small diffraction peaks observed. This was determined to be crystalline α-$Ca_2P_2O_7$. After re-melting and casting this devitrification was not observed, due to the faster cooling during casting preventing crystallisation.

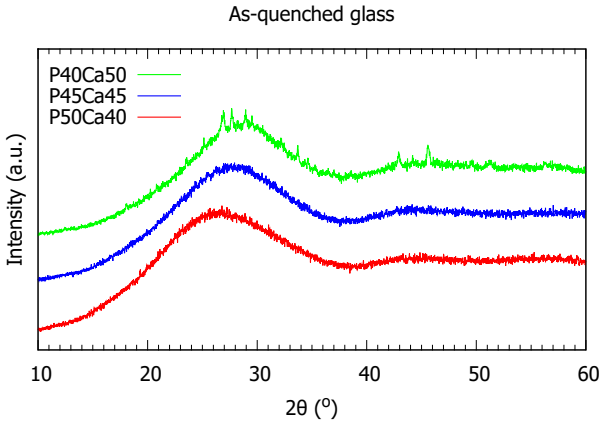

Figure S1: XRD patterns for as-quenched phosphate glasses. Patterns are offset vertically for clarity.

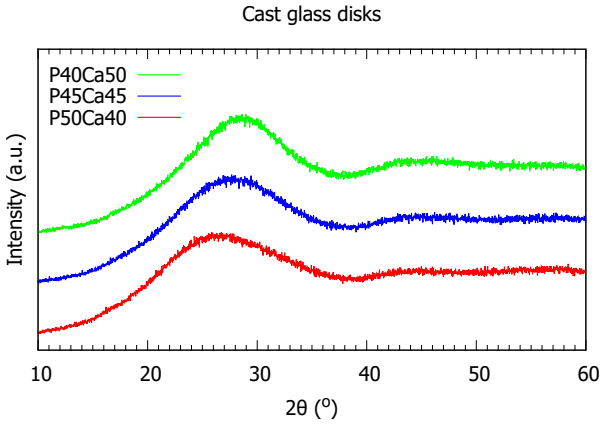

Figure S2: XRD patterns for cast phosphate glass discs. Patterns are offset vertically for clarity.

NMR spectroscopy was carried out on the phosphate glasses in their as-quenched state, before re-melting and casting. These spectra and their deconvolutions are shown in Fig. S3, with fitted peaks assigned to specific chemical shifts with reference to literature [29–31]. Q^1 and Q^2 phosphate tetrahedra were observed,

with the proportion of Q^1 tetrahedra increasing as more Ca was added to the glass. The high calcium P40Ca50 glass also displayed two small peaks attributed to the crystalline α-$Ca_2P_2O_7$. XRD measurements determined that this devitrified material was not present in the cast disks, so the cast disks can be assumed to consist solely of Q^1 and Q^2 phosphate tetrahedra.

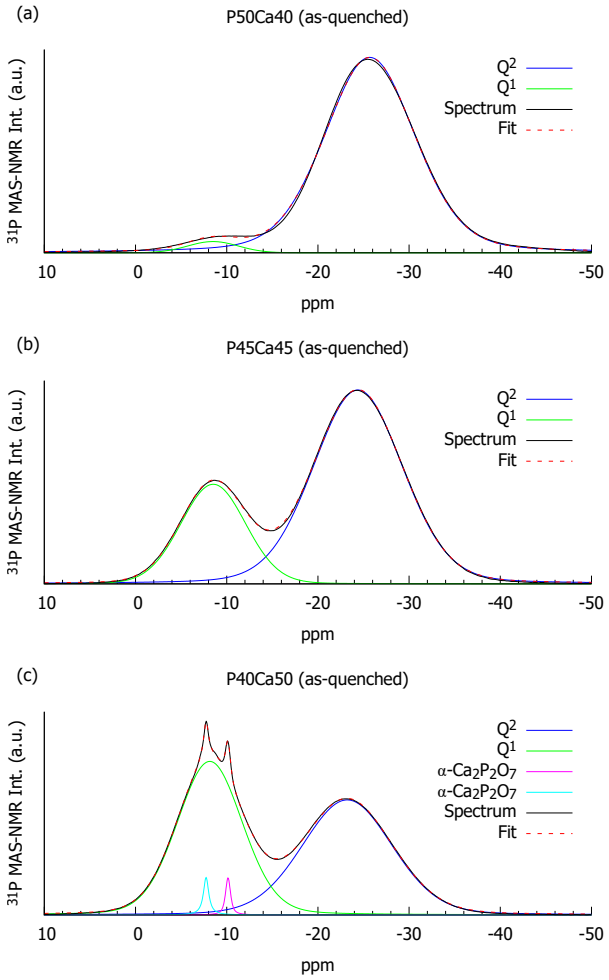

Figure S3: ^{31}P MAS-NMR spectra of as-quenched phosphate glasses, showing measured spectra and fitted peaks.

FTIR (Fourier Transform Infrared Spectroscopy) was carried out on phosphate glass samples using a Bruker Tensor 27 FTIR Spectrometer, in ATR configuration (Attenuated Total Reflectance). These spectra are shown in Fig. S4. A background scan was obtained before each sample scan, and three replicates were analysed for each sample. Spectra were collected over the range 520 - 4000 cm^{-1}, with a resolution of 8 cm^{-1}, and 16 scans were collected for each sample.

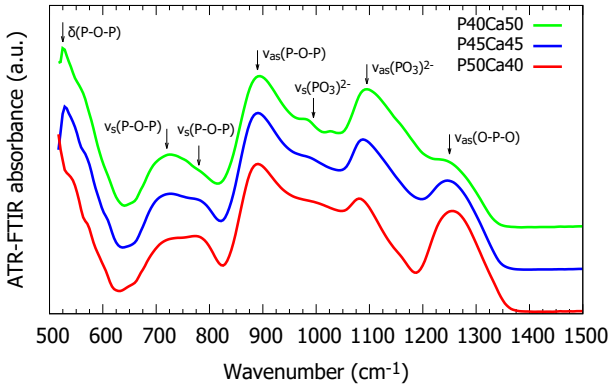

Figure S4: ATR-FTIR spectra of the phosphate glasses used, with peak assignments shown.

S.2. ISE Calibration

A typical calibration curve for the calcium ISE is shown in Fig. S5. Calibration standards were measured twice, the second time in reverse order, to minimise potential drift and hysteresis during measurement. The average of these values was used to fit the calibration curve. A modified Nernst equation was fitted to account for reagent blank determinand as well as interference at low concentration, which occurs with all electrodes [25]. Calibration was repeated before measurement of each new timepoint, and the electrode was cleaned if the slope (S_1) deviated significantly (>2 mV) from the theoretical value of 29.6 mV/decade at 25°C.

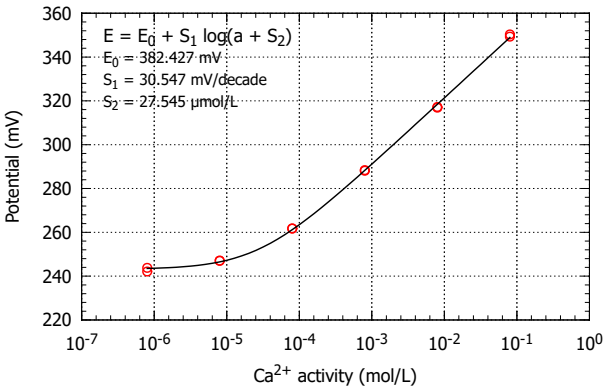

Figure S5: Typical calibration curve for calcium ISE, using Hanna HI 4004-01 calcium standard.

Table S1: Fitted reaction rate parameters for two-stage models for phosphate glass dissolution.

Glass code	Solution	k_{DM} (μm/day$^{0.5}$)	k_{CVM} (μm/day)	t_{trans} (days)	R^2
P50Ca40	DI H_2O	-	19.4 (±0.3)	< 0.04	0.999
P45Ca45	DI H_2O	3.5 (±0.1)	0.224 (±0.003)	4.9 (±0.5)	0.989
P40Ca50	DI H_2O	1.52 (±0.02)	0.041 (± 0.002)	13.2 (±0.7)	0.982
P50Ca40	PBS pH 7	6.0 (±0.3)	0.78 (±0.2)	7 (±3)	0.963
P45Ca45	PBS pH 7	3.9 (±0.3)	0.51 (±0.02)	7 (±4)	0.938
P40Ca50	PBS pH 7	2.52 (±0.06)	0.032 (±0.005)	9.3 (±0.6)	0.873
P50Ca40	PBS pH 5	14.9 (±0.3)	1.26 (±0.06)	22 (±7)	0.970
P45Ca45	PBS pH 5	8.2 (±0.4)	1.06 (±0.02)	6 (±2)	0.983
P40Ca50	PBS pH 5	5.1 (±0.1)	0.24 (±0.01)	10.2 (±0.8)	0.959
P50Ca40	PBS pH 3	34.8 (±0.8)	4.0 (±0.2)	19.4 (±0.6)	0.971
P45Ca45	PBS pH 3	37.2 (±0.5)	1.04 (±0.08)	17.2 (±0.8)	0.973
P40Ca50	PBS pH 3	24.0 (±0.5)	1.12 (±0.05)	10.5 (±0.8)	0.964

S.3. Dissolution model parameters

Published journal article:
https://doi.org/10.1016/j.jeurceramsoc.2020.08.076